Sharif University of Technology

**Scientia Iranica**

*Transactions on Civil Engineering*

https://scientiairanica.sharif.edu

# Accuracy and stability of a proposed implicit time integration method ($\zeta$-method) based on a sinusoidal interpolation function for acceleration

Soroosh Kamali [a,b], Seyed Mehdi Dehghan [a,*], Mohammad Amir Najafgholipour [a], Mohammad Ali Hadianfard [a]

*a. Department of Civil and Environmental Engineering, Shiraz University of Technology, Shiraz, Iran.*
*b. Department of Civil, Chemical, Environmental, and Materials Engineering (DICAM), University of Bologna, University of Bologna, Bologna, Italy.*

* Corresponding author: smdehghan@sutech.ac.ir (S.M. Dehghan)

Received 22 March 2022; received in revised form 8 March 2023; accepted 20 June 2023

**Keywords**

Numerical time integration methods;
Stability analysis;
Accuracy analysis;
Optimization;
Spectral radius.

**Abstract**

In this paper, the accuracy and stability of an implicit numerical method ($\zeta$-method) is investigated. It is shown that $\zeta$-method presents high accuracy and efficiency for the dynamic response analysis by assuming a sinusoidal interpolation function for acceleration between two successive time steps. Assuming a sinusoidal distribution of acceleration results in similar types of equations for velocity and displacement since the integration of a sine term contains sine and cosine terms. For this method, a parameter (denoted as $\zeta$) is used as the frequency of the sinusoidal interpolation function which significantly affects the accuracy and stability of the method. The equations and derivations are presented in detail and the best value for $\zeta$ is obtained through multi-objective optimization procedures to minimize the errors. The accuracy and stability of the method have been investigated in terms of period elongation, amplitude decay, and spectral radius. Finally, the method has been evaluated by several numerical examples (linear and nonlinear Single-Degree-of-Freedom (SDOF), and linear Multi-Degree-of-Freedom (MDOF)). In some examples, it was observed that the $\zeta$-method yielded better results than other numerical methods. Moreover, an interpolated version of the method was introduced which was more accurate in comparison with similar methods with equal execution time.

## 1. Introduction

Time integration methods are numerical techniques that use some approximations and assumptions to solve the governing differential equation at each time step when the response history of a system is of interest. They are divided into implicit and explicit groups. In implicit methods, the governing differential equation at time step $i + 1$ is used to find the response of the $i$th time step. In explicit methods, the governing differential equation at time step $i$ is used [1]. For time integration methods, there are key points required to investigate such as accuracy, stability, and consistency. Accuracy is usually defined as period elongation and amplitude decay, i.e., the obtained periods and amplitudes are greater or smaller, compared to the exact solutions. Stability is a criterion representing whether the cumulative errors at successive time steps cause unbounded solutions or not. Some of the time integration methods are unconditionally stable which is desirable, i.e., no matter what the time step is, the response is always bounded. Consistency is another requirement for any time integration method to be convergent. It is evaluated by calculating local truncation error, which is the difference between the actual solution and the numerical solution at one time step.

Several researchers have proposed different time integration methods. Each method has some advantages and some disadvantages in terms of stability, accuracy, and consistency. In 1950, Houbolt's method was introduced as an implicit method to solve the response of an airplane subjected to dynamic loads [2]. This method is

**To cite this article:**
S. Kamali, S.M. Dehghan, M.A. Najafgholipour, M.A Hadianfard "Accuracy and stability of a proposed implicit time integration method (ζ-method) based on a sinusoidal interpolation function for acceleration", *Scientia Iranica* (2025) **32**(7): 6637 https://doi.org/10.24200/sci.2023.60165.6637

unconditionally stable, while it has greater amplitude decays and period elongations compared to up-to-dated methods. In 1959, Newmark proposed an implicit method based on the two constants $\beta$ and $\gamma$ representing the different interpolation functions of acceleration. Newmark's method has shown a satisfactory performance from the stability and accuracy viewpoints and is vastly used in structural dynamics [3]. Two famous formulations of Newmark's method are linear acceleration and average acceleration. The former shows higher accuracy while the latter is unconditionally stable. Wilson's [4] implicit method was introduced in 1972. The method is a step-by-step technique to evaluate the dynamic response of structures with physical and geometrical nonlinearities. The method was stable for all time steps introducing a predictable error for a specified time step. In 2010, Leontyev proposed the two-step Lambda method with controllable numerical dissipation [5]. The method is an unconditionally stable implicit Level Symmetric (LS) method which results in strong dissipation of high-frequency modes. In 2012, Bathe and Noh [6] proposed a useful implicit time integration method for linear and nonlinear systems and presented its accuracy, stability, and spectral radius. They examined their proposed method through a very flexible and a very stiff system, getting superior results for both cases. Later, they added further insights to their method by using the parameter "time step splitting ratio" and showed that by changing this parameter, they can obtain large amplitude decays which might be desirable for some problems [7].

In 2014, Wen et al. [8] proposed an explicit numerical method based on the interpolation polynomial functions of septuple B-spline and investigated its stability and accuracy. By use of adjustable parameters, they showed that a high-frequency response can be damped out without inducing excessive algorithmic damping in important low frequency modes. In 2015, Wen et al. [9] suggested a novel time integration method by employing uniform quintic B-spline polynomial interpolation. As a result, using two adjustable parameters, the method was formulated for solving the differential equation of motion governing a Single-Degree-of-Freedom (SDOF) system and then, was generalized for a Multi-Degree-of-Freedom (MDOF) system. The proposed method not only had higher computation efficiency but also possessed better numerical dissipation characteristics. In 2013, Rostami et al. [10] proposed an explicit time integration method for structural dynamics using cubic B-spline polynomial functions for MDOF systems. This method was conditionally stable, it was faster, but had the same accuracy as the Newmark linear acceleration method. Later in 2015, Shojaee et al. [11] presented an unconditionally stable numerical method as a modified quartic B-spline method which had good accuracy with lower period elongation and amplitude decay. In 2015, Muradova [12] proposed a time spectral method for solving the nonlinear dynamic equations of a rectangular elastic plate. They used the Runge–Kutta method and the Newmark-$\beta$ method to solve the nonlinear ordinary differential equations. In 2016, Ding et al. [13] proposed a state-space-based method to solve structural dynamics problems with multiple non-viscous damping models. They obtained better results in terms of accuracy and efficiency compared to some implicit methods. In 2012, Hadianfard [14] used the integrated displacement method to improve the step-by-step nonlinear response of the structure. Their proposed method permitted longer time steps and reduced computational costs.

In 2017, Wen et al. [15] presented an implicit sub-step composite method. Their method had good accuracy, stability, numerical dissipation/dispersion characteristics, and computational efficiency and showed a good performance in wave propagation analysis. In 2017, Zhang et al. [16] studied an implicit two-sub-step composite time integration method for the dynamics of structures. They also evaluated the truncation errors of the response parameters with a systematic procedure. Kwon and Lee [17] proposed a time integration scheme in 2017 to solve problems dealing with stress wave propagation. Their method presented non-oscillatory solutions for such problems.

In 2018, Xing et al. [18] proposed a strategy to construct a highly accurate and efficient time integration method for linear time-invariant systems. They employed the multi-sub-step notion and reduced the rounding errors and the computational costs. In 2018, Kim and Choi [19] developed an improved implicit time integration method using the weighted residual method. Their method enjoys algorithmic dissipation control, can also be used for nonlinear systems, and represented improved results in comparison with Bathe method.

In 2019, Zhang and Xing [20] proposed two explicit methods based on displacement-velocity relations for the dynamics of structures. The method presents second-order accuracy with good stability and performed better for some numerical examples in comparison with some up-to-date explicit methods. In 2019, Yuan et al. presented a highly accurate and efficient explicit time integration method for typical problems of structural dynamics. They used optimization to find the best values of the parameters they defined in their method [21]. Their proposed method has second-order consistency, with a superior stability limit while damping exists. They got better computational efficiency in comparison with the up-to-date methods in their literature. In 2019, Kim [22] proposed a single-step explicit numerical method based on the Newmark approximations and verified its performance by linear and non-linear examples. Their method is second-order consistent for linear and nonlinear velocity dependent systems and could present slightly better results compared to existing methods. In 2020, Kim and Reddy [23] developed four sets of two-stage explicit numerical methods using truncated Taylor's series expansions of displacement and velocity. They obtained an improved order of consistency as three of their schemes had much smaller period elongations compared with any existing time-integration method. In 2019, Noah and Bathe [24] proposed the sub-step $\rho_\infty$-Bathe method with controllable spectral radius. Their goal was to prescribe the period

elongation and amplitude decay in an optimum manner. With controllable spectral radius and time splitting ratio, they showed that it is possible to have zero to very large period elongations, and correspondingly small to very large amplitude decays while keeping the second-order consistency. In 2019, Malakiyeh et al. [25] used the 3-point trapezoidal rule for the complete step for the second sub-step and used two parameters to prescribe numerical dissipation of interest for Bathe method. They proved that with proper constants, it is possible to obtain the best accuracy in the lowest modes integration and a quick suppression of spurious response in the higher modes of the system. In 2020, Li and Yu [26] proposed a family of composite sub-step algorithms with controllable numerical dissipations. Their proposed method is a sub-step method, unconditionally stable, and its computational cost is the same as the Bathe algorithm. In 2021, Nguyen et al. [27] developed efficient and accurate numerical algorithms to solve a generalized Kirchhoff–Love plate model subject to three common physical boundary conditions. More examples of the implicit methods can be found in [28-32] and some examples of the explicit methods are presented in [33-35].

In this paper, a highly accurate and efficient implicit time integration method has been introduced which is based on a sinusoidal interpolation function of acceleration between two successive time steps. The method has been named based on the frequency ($\zeta$) of the sinusoidal function. Firstly, the formulation of the method is introduced, and the corresponding equations and relations are derived step-by-step for SDOF systems, and then generalized for MDOF systems. In this paper, the linear form of the system is considered, and then is verified for nonlinear systems through an example. Next, the stability and accuracy of the method are theoretically and numerically investigated, and its spectral radius (as the stability criterion) is calculated and compared with those of other methods. Using a multi-objective optimization, the best value of $\zeta$ is obtained by minimizing the errors in accuracy. Moreover, numerical examples are solved using the $\zeta$-method and the results are compared with the responses of other time integration methods.

## 2. Formulation of $\zeta$-method

This method assumes a sinusoidal variation of the response acceleration between two successive time steps. In other words, the interpolation function between the two-time steps is a sinusoidal function expressed as:

$$\ddot{u}(\tau) = \ddot{u}_i + A\sin(\zeta\tau), \tag{1}$$

where $\ddot{u}_i$ is the response step $i$, $\zeta$ is the acceleration at time circular frequency of the acceleration interpolation function, $A$ is the coefficient of the sine term, and $\tau$ represents the time between two successive time steps. As a result, at $t_i$, $\tau = 0$ and at $t_{i+1}$, $\tau = \Delta t$ ($\Delta t$ is the time step) (Figure 1). If $\tau = \Delta t$, then:

$$\ddot{u}_{i+1} = \ddot{u}_i + A\sin(\zeta\Delta t). \tag{2}$$

Rearranging Eq. (2), results in:

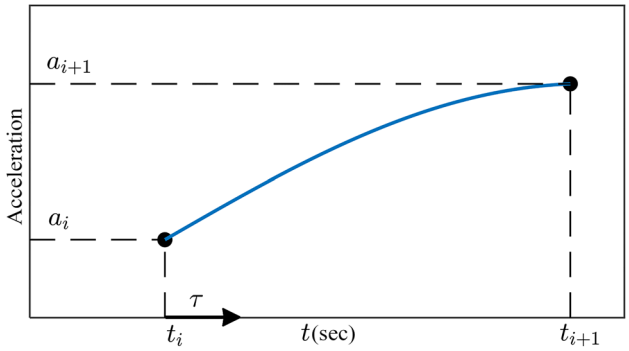


**Figure 1.** Sinusoidal interpolation of acceleration between two successive time steps with respect to $\tau$.

$$A = \frac{\ddot{u}_{i+1} - \ddot{u}_i}{\sin(\zeta\Delta t)}. \tag{3}$$

Substituting Eq. (3) into Eq. (1) leads to:

$$\ddot{u}(\tau) = \ddot{u}_i + \frac{\ddot{u}_{i+1} - \ddot{u}_i}{\sin(\zeta\Delta t)}\sin(\zeta\tau). \tag{4}$$

The integration of Eq. (4) yields the velocity between the two-time steps as:

$$\dot{u}(\tau) = \dot{u}_i + \ddot{u}_i\tau - \frac{\ddot{u}_{i+1} - \ddot{u}_i}{\zeta\sin(\zeta\Delta t)}\cos(\zeta\tau). \tag{5}$$

At time instant $\tau = \Delta t$, the velocity can be obtained as follows:

$$\dot{u}_{i+1} = \dot{u}_i + \ddot{u}_i\Delta t - \frac{\ddot{u}_{i+1} - \ddot{u}_i}{\zeta\tan(\zeta\Delta t)} \tag{6}$$

In order to derive the displacement equation between the two-time steps, Eq. (5) is integrated:

$$u(\tau) = u_i + \dot{u}_i\tau + \ddot{u}_i\frac{\tau^2}{2} - \frac{\ddot{u}_{i+1} - \ddot{u}_i}{\zeta^2\sin(\zeta\Delta t)}\sin(\zeta\tau). \tag{7}$$

At time instant $\tau = \Delta t$, the displacement can be obtained as follows:

$$u_{i+1} = u_i + \dot{u}_i\Delta t + \ddot{u}_i\frac{\Delta t^2}{2} - \frac{\ddot{u}_{i+1} - \ddot{u}_i}{\zeta^2} \tag{8}$$

Rearranging Equation (8) to find $\ddot{u}_{i+1}$ results in:

$$\ddot{u}_{i+1} = \zeta^2 u_i - \zeta^2 u_{i+1} + \zeta^2\Delta t\dot{u}_i + \left(\frac{\zeta^2\Delta t^2}{2} + 1\right)\ddot{u}_i. \tag{9}$$

By substituting Eq. (9) into Eq. (6) and rearranging the equations, we have :

$$\dot{u}_{i+1} = \dot{u}_i + \ddot{u}_i\Delta t + \frac{\ddot{u}_i}{\zeta\tan(\zeta\Delta t)} - \frac{1}{\zeta\tan(\zeta\Delta t)}\left[\zeta^2 u_i - \zeta^2 u_{i+1} + \zeta^2\Delta t\dot{u}_i + \left(\frac{\zeta^2\Delta t^2}{2} + 1\right)\ddot{u}_i\right],$$

$$\dot{u}_{i+1} = \dot{u}_i + \ddot{u}_i\Delta t + \frac{\ddot{u}_i}{\zeta\tan(\zeta\Delta t)} - \frac{\zeta^2 u_i}{\zeta\tan(\zeta\Delta t)} + \frac{\zeta^2 u_{i+1}}{\zeta\tan(\zeta\Delta t)} - \frac{\zeta^2\Delta t\dot{u}_i}{\zeta\tan(\zeta\Delta t)} - \frac{\zeta^2\Delta t^2\ddot{u}_i}{2\zeta\tan(\zeta\Delta t)} - \frac{\ddot{u}_i}{\zeta\tan(\zeta\Delta t)},$$

$$\dot{u}_{i+1} = -\frac{\zeta}{\tan(\zeta\Delta t)}u_i + \frac{\zeta}{\tan(\zeta\Delta t)}u_{i+1} + \dot{u}_i - \frac{\zeta}{\tan(\zeta\Delta t)}\Delta t\dot{u}_i - \frac{\zeta}{2\tan(\zeta\Delta t)}\Delta t^2\ddot{u}_i + \Delta t\ddot{u}_i. \quad (10)$$

Taking $\gamma = \frac{\zeta}{\tan(\zeta\Delta t)}$:

$$\dot{u}_{i+1} = -\gamma u_i + \gamma u_{i+1} + (1-\gamma\Delta t)\dot{u}_i + \left(\Delta t - \frac{\gamma\Delta t^2}{2}\right)\ddot{u}_i. \quad (11)$$

By considering the implicit scheme, the equation of motion at each time step can be written as follows:

$$m\ddot{u}_{i+1} + c\dot{u}_{i+1} + ku_{i+1} = P_{i+1}. \quad (12)$$

If Eqs. (9) and (11) are employed for $\ddot{u}_{i+1}$ and $\dot{u}_{i+1}$, respectively, Eq. (12) can be rewritten as:

$$m\left[\zeta^2 u_i - \zeta^2 u_{i+1} + \zeta^2\Delta t\dot{u}_i + \left(\frac{\zeta^2\Delta t^2}{2}+1\right)\ddot{u}_i\right] + c\left[-\gamma u_i + \gamma u_{i+1} + (1-\gamma)\Delta t\dot{u}_i + \left(\Delta t - \frac{\gamma\Delta t^2}{2}\right)\ddot{u}_i\right] + ku_{i+1} = P_{i+1},$$

$$\left[-m\zeta^2 + c\gamma + k\right]u_{i+1} + \left[m\zeta^2 - c\gamma\right]u_i + \left[m\zeta^2\Delta t - c\gamma\Delta t + c\right]\dot{u}_i + \left[\frac{m\zeta^2\Delta t^2}{2} + m + c\Delta t - \frac{c\zeta\Delta t^2}{2}\right]\ddot{u}_i = P_{i+1}. \quad (13)$$

By introducing the following constants:

$$a_1 = \left[-m\zeta^2 + c\gamma + k\right],$$
$$a_2 = \left[m\zeta^2 - c\gamma\right],$$
$$a_3 = \left[m\zeta^2\Delta t - c\gamma\Delta t + c\right],$$
$$a_4 = \left[\frac{m\zeta^2\Delta t^2}{2} + m + c\Delta t - \frac{c\gamma\Delta t^2}{2}\right]. \quad (14)$$

Eq. (13) can be summarized as:

$$a_1u_{i+1} + a_2u_i + a_3\dot{u}_i + a_4\ddot{u}_i = P_{i+1}. \quad (15)$$

Rearranging Eq. (15), $u_{i+1}$ is obtained as follows [1]:

$$u_{i+1} = \frac{P_{i+1} - a_2u_i - a_3\dot{u}_i - a_4\ddot{u}_i}{a_1}. \quad (16)$$

By obtaining $u_{i+1}$, $\dot{u}_{i+1}$ can be calculated using Eq. (11). On the other hand, $\ddot{u}_{i+1}$ can be calculated using either Eq. (9) or the following equation which is a rearrangement of Eq. (12):

$$\ddot{u}_{i+1} = \frac{P_{i+1} - c\dot{u}_{i+1} - ku_{i+1}}{m}. \quad (17)$$

## 3. Stability analysis

Approximations cause errors in numerical solutions while using time integration methods. The error at each time step has some effects on the calculations of the next time step. Sometimes, the error grows cumulatively, and the solution becomes unbounded. In this case, it is said that the method is unstable.

The stability of a numerical method is examined under undamped free vibration conditions. This is because undamped vibration conditions are more restrictive than damped vibration conditions from the stability point of view (i.e., damping helps limit the response). Moreover, if a numerical method is unstable in free vibration conditions, it tends to be unstable in forced vibration conditions as well. This is since an unstable complementary solution of the differential equation will quickly make the total solution unstable.

To investigate the stability of the $\zeta$-method, it is a good practice to find a relationship between the displacement, velocity, and acceleration at time step $i+1$ and those at time step $i$. In most of the time integration methods, this can be performed by defining a matrix $\boldsymbol{A}$ which relates the response parameters at the two successive time steps as follows [36]:

$$\overrightarrow{D_{i+1}} = \boldsymbol{A}\overrightarrow{D_i},$$
$$\overrightarrow{D_{i+1}} = \left[u_{i+1}, \Delta t\dot{u}_{i+1}, \Delta t^2\ddot{u}_{i+1}\right]^T,$$
$$\overrightarrow{D_i} = \left[u_i, \Delta t\dot{u}_i, \Delta t^2\ddot{u}_i\right]^T, \quad (18)$$

where $\boldsymbol{A}$ is the amplification matrix, $\Delta t$ is the time step, and $u_{i+1}$, $\dot{u}_{i+1}$, and $\ddot{u}_{i+1}$ are displacement, velocity, and acceleration at time step $i+1$, respectively. $u_i$, $\dot{u}_i$, and $\ddot{u}_{i_i}$ are the corresponding values at time step $i$. By writing Eq. (18) at time steps $i+1$, $i$, $i-1$, and $i-2$, the following equation can be obtained:

$$u_{i+1} - 2\alpha_1u_i + \alpha_2u_{i-1} - \alpha_3 = 0, \quad (19)$$

where $\alpha_1$ is half of the trace of matrix $\boldsymbol{A}$, $\alpha_2$ is the sum of the principal minors of matrix $\boldsymbol{A}$, and $\alpha_3$ is its determinant. The solution to Eq. (19) has the following form:

$$u_i = c\lambda^i, \quad (20)$$

where the $\lambda$s are the eigenvalues of matrix $\boldsymbol{A}$ and $c$ is a constant. Substituting Eqs. (20) into (19), we have:

$$\lambda^3 - 2\alpha_1\lambda^2 + \alpha_2\lambda - \alpha_3 = 0 \quad (21)$$

which has 3 roots. Thus, the general solution can be written as:

$$u_i = \sum_{n=1}^{3} c_n\lambda_n^i. \quad (22)$$

To check the stability of the method, the undamped free vibration of the system is taken as the criterion [36]. Thus, the equation of motion can be rewritten as:

$$\ddot{u}_{i+1} + \omega^2u_{i+1} = 0, \quad (23)$$

where $\omega = \sqrt{k/m}$ is the undamped natural frequency of the system. Eq. (23) can be written in the form of Eq. (18) by employing Eqs. (6) and (8) for displacement and velocity, respectively. Thus, matrix $\boldsymbol{A}$ is obtained for the $\zeta$-method as:

$$\boldsymbol{A}=\frac{1}{\zeta^2-\omega^2}\begin{bmatrix}\zeta^2 & \zeta^2 & \dfrac{\zeta^2\Delta t^2+2}{2\Delta t^2}\\ \dfrac{\zeta\Delta t\omega^2}{\tan\zeta\Delta t} & \zeta^2-\omega^2+\dfrac{\zeta\Delta t\omega^2}{\tan\zeta\Delta t} & \zeta^2-\omega^2+\dfrac{2\zeta+\zeta\Delta t^2\omega^2}{2\Delta t\tan\zeta\Delta t}\\ -\zeta^2\Delta t^2\omega^2 & -\zeta^2\Delta t^2\omega^2 & -\dfrac{\omega^2\left(\zeta^2\Delta t^2+2\right)}{2}\end{bmatrix} \quad (24)$$

Thus, the determinant, half of the trace, and the sum of the principal minors of matrix $\boldsymbol{A}$ are given by:

$$\begin{aligned}\alpha_1&=1+\frac{1}{\zeta^2-\omega^2}\left[\frac{\zeta\Delta t\omega^2}{2\tan\zeta\Delta t}-\frac{\zeta^2\Delta t^2\omega^2}{4}\right],\\ \alpha_2&=1+\frac{1}{\zeta^2-\omega^2}\left[\frac{\zeta\Delta t\omega^2}{\tan\zeta\Delta t}+\frac{\zeta^2\Delta t^2\omega^2}{2}\right],\\ Det\left(\boldsymbol{A}\right)&=\alpha_3=0.\end{aligned} \quad (25)$$

With $\alpha_3=0$, Eq. (21) can be expressed as:

$$\lambda^2-2\alpha_1\lambda+\alpha_2=0. \quad (26)$$

The roots of the preceding equation are:

$$\lambda_{1,2}=\alpha_1\pm\sqrt{\alpha_1^2-\alpha_2}. \quad (27)$$

According to Eq. (22), to have an oscillatory motion, $\alpha_1^2-\alpha_2$ must be negative [36]:

$$\alpha_1^2-\alpha_2<0. \quad (28)$$

which gives one stability condition. On the other hand, Eq. (27) can be presented as:

$$\lambda_{1,2}=\alpha_2^{1/2}(\cos\phi\pm i\sin\phi), \quad (29)$$

where $i=\sqrt{-1}$ and:

$$\tan\phi=\pm\sqrt{\frac{\alpha_2-\alpha_1^2}{\alpha_1}}. \quad (30)$$

Substituting Eq. (29) into (22), the following equation is obtained for the response:

$$u_i=\alpha_2^{i/2}(c_1\cos i\,\phi+c_2\sin i\,\phi), \quad (31)$$

where $c_1$ and $c_2$ are determined from the initial conditions and $i$ stands for the numbers of the time steps. By increasing $i$, $\alpha_2^{i/2}$ approaches infinity if $\alpha_2>1$. As a result, for the amplitude to remain limited, the stability condition must be $\alpha_2\le 1$. To summarize, the condition for a stable oscillation is:

$$\alpha_1^2<\alpha_2\le 1. \quad (32)$$

To satisfy condition (28), by considering the values of $\alpha_1$ and $\alpha_2$ obtained from Eq. (25), the following inequality must be valid:

$$\frac{\zeta^2\Delta t^2\omega^2}{\left(\zeta^2-\omega^2\right)^2}\left[\frac{\omega^2}{4\tan^2\zeta\Delta t}-\frac{\zeta\Delta t\omega^2}{4\tan\zeta\Delta t}+\frac{\zeta^2\Delta t^2\omega^2}{16}+\omega^2-\zeta^2\right]<0. \quad (33)$$

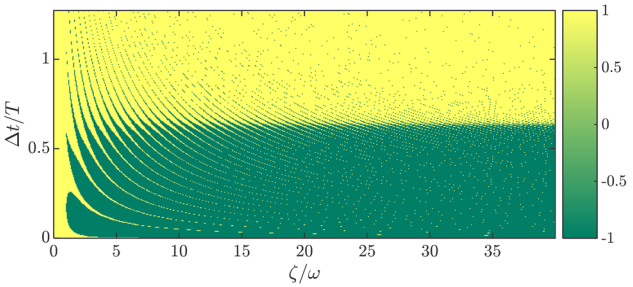


**Figure 2.** Sign of $F(x, y)$ for the sample space.

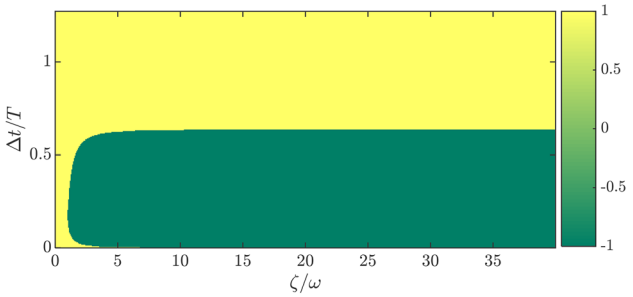


**Figure 3.** Sign of $F(x, y)$ using Taylor expansion approximation for the sample space.

Firstly, the following conditions must be satisfied:

$$\begin{aligned}&\zeta\neq\omega,\\ &\zeta\Delta t\neq\frac{(2n-1)\pi}{2},\qquad n=1,\,2,\,3,\,\cdots,\end{aligned} \quad (34)$$

By factoring the $\omega^2$ term in the bracket and dividing Eq. (33) by $\omega^2\frac{\zeta^2\Delta t^2\omega^2}{(\zeta^2-\omega^2)^2}$, we will have:

$$\frac{1}{4\tan^2\zeta\Delta t}-\frac{\zeta\Delta t}{4\tan\zeta\Delta t}+\frac{\zeta^2\Delta t^2}{16}+1-\frac{\zeta^2}{\omega^2}<0. \quad (35)$$

Let $x=\zeta/\omega$ and $y=\Delta t/T$ $(T=2\pi/\omega)$. Then, Eq. (35) can be rewritten as:

$$\begin{aligned}F\left(x,y\right)=&\frac{1}{4\tan^2 2\pi xy}-\frac{2\pi xy}{4\tan 2\pi xy}+\frac{\left(2\pi\right)^2x^2y^2}{16}\\ &+1-x^2<0.\end{aligned} \quad (36)$$

The solution to the preceding inequality might be obtained. The value of sign $[F(x,\,y)]$ is calculated for several values of $x$ and $y$ as plotted in Figure 2. To provide a better view, $\tan x\,y$ is expanded using the first four terms of the Taylor expansion as:

$$\tan x\,y\simeq xy+\frac{x^3y^3}{3}+\frac{2x^5y^5}{15}+\frac{17x^7y^7}{315}. \quad (37)$$

The same process is performed to obtain the plot of sign $[F(x,\,y)]$ using the Taylor approximation, as shown in Figure 3. It can be observed that there is no sign of discontinuities in this Figure in contrast to Figure 2. The discontinuities in Figure 2 are due to ignoring condition (34) in the selection of $x$ and $y$. In addition to condition (34), based on Figure 3, an approximate stability condition for $y$ and $x$ can be stated as:

$$y = \frac{\Delta t}{T} < 0.6, \qquad x = \frac{\zeta}{\omega} > 5. \tag{38}$$

To satisfy $\alpha_2 \leq 1$ in condition (32), Eq. (25) is rewritten as:

$$1 + \frac{\omega^2 \zeta \Delta t}{\zeta^2 - \omega^2}\left[cot\,\zeta\,\Delta t + \frac{\zeta \Delta t}{2}\right] \leq 1. \tag{39}$$

Since $\zeta$ is positive, by rearranging the inequality, the condition is reduced to:

$$cot\,\zeta\,\Delta t \leq -\frac{\zeta \Delta t}{2}. \tag{40}$$

Thus, as the stability criterion, the selected $\zeta \Delta t$ must satisfy condition (40). Stability conditions are essential to have an oscillatory motion and ensure that the motion stays bounded. However, the accuracy of the response might not be guaranteed.

## 4. Accuracy analysis

Accuracy is an important parameter in selecting a time integration method. Under the critical free vibration conditions, accuracy can be investigated from two viewpoints: errors in amplitude and period. In other words, the amplitude or period obtained by the time integration method might be different from the actual values. To investigate these errors, Eq. (20) can be rewritten as follows [36]:

$$u_i = c_1 \lambda_1^i + c_2 \lambda_2^i. \tag{41}$$

$\lambda_1$ and $\lambda_2$ are in the form of $m + ni$ and $m - ni$ and have been calculated in Eq. (27). Thus, Eq. (41) can be written as:

$$u_i = \lambda_p (c_1' \cos \omega' \tau_i + c_2' \sin \omega' \tau_i), \tag{42}$$

where $\lambda_p = \sqrt{m^2 + n^2}$, $\phi = tann/m^{-1}$, $\omega' = \phi/\Delta t$, $\tau_i = i\Delta t$, and $i$ indicates the numbers of the time steps. To obtain the exact solution and to observe no amplitude change with $i$, $\lambda_p$ must be equal to unity. Since this is not practical in time integration methods, an amplitude decay and a period elongation are defined as follows [36]:

$$PE = \frac{T' - T}{T} = \frac{\omega \Delta t - \phi}{\phi}, \tag{43}$$

$$AD = 1 - \lambda_p^{\frac{2\pi}{\phi}}. \tag{44}$$

where $T' = 2\pi/\omega'$ and $\omega$ is the natural circular frequency of the system. The spectra of the period elongation and amplitude decay of the $\zeta$-method for different values of $\zeta/\omega$ and $\Delta t/T$ are plotted in Figures 4 and 5, respectively. In these figures, the horizontal and vertical axes represent $\zeta/\omega$ and $\Delta t/T$ ratios, respectively. The colors in the images show the intensity of the AD or PE parameters expressed in the color bar. It can be concluded that the accuracy of the $\zeta$-method is unacceptable for $\Delta t/T > 0.3$. However, this is not a limitation while dealing with a time history analysis since small $\Delta t/T$s are usually used for modeling the time history in typical problems. In addition, there is a wide range of $\zeta$

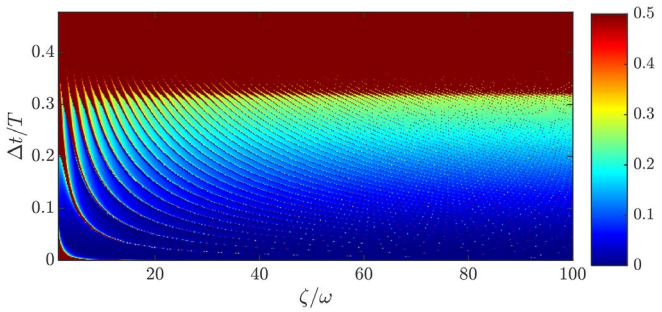


**Figure 4.** Period elongation of the $\zeta$-method.

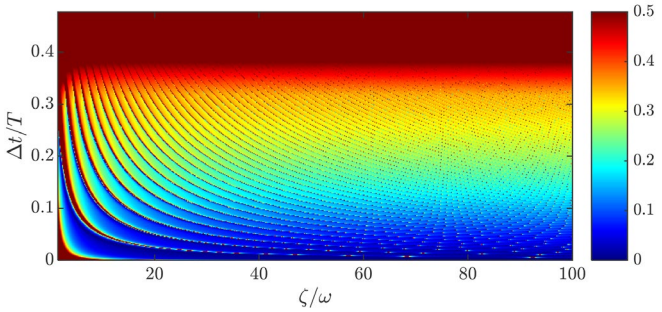


**Figure 5.** Amplitude decay of the $\zeta$-method.

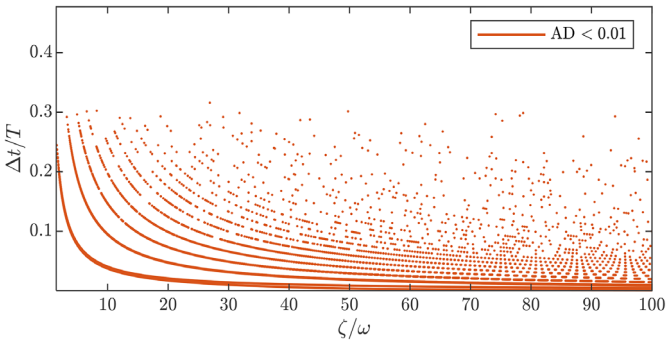


**Figure 6.** Contours corresponding to the amplitude decays of less than 0.01.

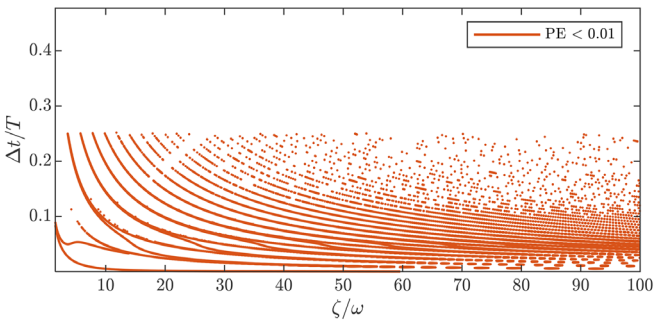


**Figure 7.** Contours corresponding to the period elongations of less than 0.01.

which can be chosen for a rather accurate result and the best value of $\zeta$ should be found among the possible values.

## 5. The best value of $\zeta$

Figures 6 and 7 show the contours of $AD < 0.01$ and $PE < 0.01$, respectively, giving a general view about the form of the relationship between $\zeta/\omega$ and $\Delta t/T$ for the points with a

**Table 1.** Curve-fitting parameters of AD < 0.01.

| *SSE* | $R^2$ | *DFE* | $R^2_{adj}$ | *RMSE* |
|---|---|---|---|---|
| **0.0166** | 0.9998 | 3279 | 0.9998 | 0.0023 |

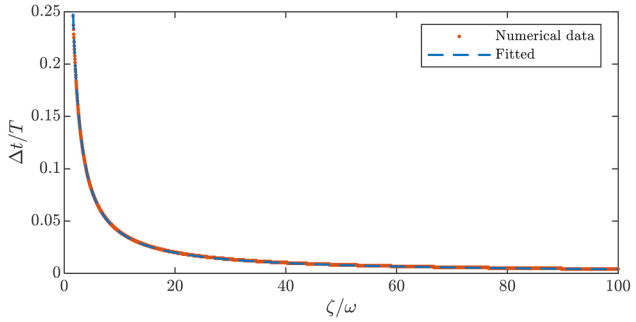


**Figure 8.** Curve fitted to the data of the first contour.

good accuracy. It seems that a homographic relationship exists between $\zeta/\omega$ and $\Delta t/T$ as follows:

$$\left(\frac{\Delta t}{T}\right) = \frac{D}{\left(\frac{\zeta}{\omega}\right)}, \tag{45}$$

where $D$ is a constant value. This hypothesis was checked for several contours of both Figures 6 and 7 using curve fitting techniques. For instance, Figure 8 was obtained for the first contour of $AD < 0.01$ with curve-fitting parameters presented in Table 1. The same process was performed for the other contours revealing the fact that Eq. (45) fits well to the data. Rearranging Equation (45) using $\omega = 2\pi/T$, the following relation was obtained for $\zeta$:

$$\zeta = \frac{C}{\Delta t}, \tag{46}$$

where $C$ is a constant value.

To find the best $C$ value, Multi-Objective Particle Swarm Optimization (MOPSO) [37] was used to minimize the errors of Eqs. (43) and (44) with $C$ as the design variable. The objective functions were defined as the summation of AD or PE for all $\Delta t/T$s in the range of 0 to 0.2 with a step of 0.01 to consider all $\Delta t/T$s for the minimization problem. From the resulting Pareto front, $C$ = 62.8 provided the best solution. The optimization settings and the best solution are presented in Table 2. Having the best value of $\zeta$, a generalized algorithm has been presented for the $\zeta$-method in Table 3 which can also be used for MDOF systems.

## 6. Stability, accuracy, and consistency

### 6.1. Spectral radius, amplitude decay, and period elongation

As an acceptable representation of the stability of a time integration method, spectral radius is defined as $\rho_s = \text{Max}(|\lambda_1|, |\lambda_2|, |\lambda_3|)$. Considering the general solution expressed as Eq. (22), if the absolute value of any $\lambda_i$ becomes larger than unity, the resulting response starts diverging and

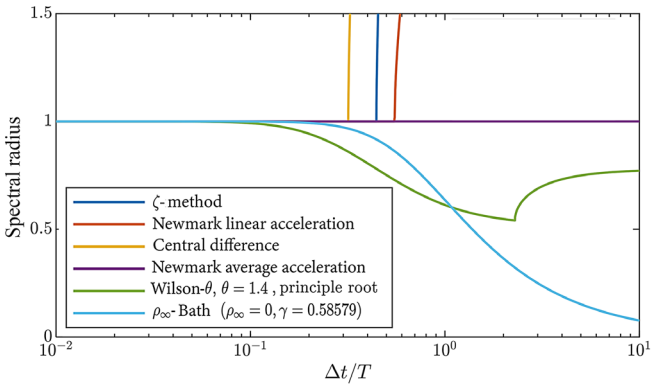


**Figure 9.** Comparing the spectral radius of the $\zeta$-method for $\zeta = 62.8/\Delta t$ with those of the other time integration methods.

the solution becomes unstable as the step-by-step numerical solution progresses. Since $\lambda_3$ is zero for the $\zeta$-method, $\rho_s = \text{Max}(|\lambda_1|, |\lambda_2|)$ and $\lambda_i$s can be calculated using Eq. (27).

It is worth mentioning that for the value of $C$ obtained from optimization, the value of $\cot \zeta \Delta t$ is equal to $-\zeta \Delta t/2$ with a negligible error. Accordingly, condition (40) is always satisfied. On the other hand, when $\cot \zeta \Delta t \simeq -\zeta \Delta t/2$, the value of $\alpha_2$ in Eq. (25) will be equal to unity. Moreover, the value of $\alpha_1$ is reduced to:

$$\alpha_1 = 1 - \frac{\zeta^2 \Delta t^2 \omega^2}{2(\zeta^2 - \omega^2)}. \tag{47}$$

This value of $\alpha_1$ is always less than unity based on condition (38). In addition, since $\alpha_2 = 1$, Inequality (28) always holds. It should be noted that condition (38) always holds for $\zeta = 62.8/\Delta t$ by taking Eq. (46) into account.

To evaluate the $\zeta$-method for $\zeta = 62.8/\Delta t$, the spectral radii of a few time integration methods have been plotted in Figure 9. It can be concluded that the $\zeta$-method with $\zeta = 62.8/\Delta t$ becomes unstable at a $\Delta t/T$ greater than that at which the central difference method becomes unstable and at a $\Delta t/T$ less than that at which the Newmark linear acceleration method becomes unstable. The spectral radius of the Newmark average acceleration method is equal to unity and the Wilson-$\theta$ method is unconditionally stable for $\theta = 1.4$. The $\zeta$-method becomes unstable for $\Delta t/T \geq 0.44$. In this figure, the constants of the $\rho_\infty$-Bathe method were $\rho_\infty = 0$ and $\gamma = \frac{2-\sqrt{2+2\rho_\infty}}{1-\rho_\infty}$ as the default values introduced in [24].

The amplitude decay and period elongation of the $\zeta$-method are plotted in Figures 10 and 11, respectively. The results show that this method has no amplitude decay. The period elongation of the $\zeta$-method is very close to that of the central difference method.

### 6.2. Local truncation error and consistency

In addition to stability, consistency is a requirement for any time integration method to be convergent. The order of consistency can be determined by calculating the local

**Table 2.** Settings and results of the multi-objective particle swarm optimization.

| Population size | Number of iterations (Generations) | Repository size | Best solution |
|---|---|---|---|
| 100 | 10000 | 100 | 62.8000167 |

**Table 3.** Algorithm of the $\zeta$-method.

| | **1. *Initial calculations**** |
|---|---|
| 1.1 | *Select* $\Delta t$ |
| 1.2 | *Take* $\zeta = 62.8/\Delta t$ |
| 1.3 | $\gamma = \frac{\zeta}{tan(\zeta \Delta t)}$ |
| 1.4 | $u_0 = [(u_0)_1.(u_0)_2.\ldots.(u_0)_N]^T$<br>$\dot{u}_0 = [(\dot{u}_0)_1.(\dot{u}_0)_2.\ldots.(\dot{u}_0)_N]^T$<br>$\ddot{u}_0 = M^{-1}(P_0 - C\dot{u}_0 - Ku_0)$ |
| 1.5 | $a_1 = [-M\zeta^2 + C\gamma + K]$ |
| 1.6 | $a_2 = [M\zeta^2 - C\gamma]$ |
| 1.7 | $a_3 = [M\zeta^2\Delta t - C\gamma\Delta t + C]$ |
| 1.8 | $a_4 = \left[M\frac{\zeta^2\Delta t^2}{2} + M + C\Delta t - C\frac{\gamma\Delta t^2}{2}\right]$ |
| | **2. *Calculations for other time steps*** |
| 2.1 | $u_{i+1} = a_1^{-1}(P_{i+1} - a_2u_i - a_3\dot{u}_i - a_4\ddot{u}_i)$ |
| 2.2 | $\dot{u}_{i+1} = -\gamma u_i + \gamma u_{i+1} + (1 - \gamma\Delta t)\dot{u}_i + \left(\Delta t - \frac{\gamma\Delta t^2}{2}\right)\ddot{u}_i$ |
| 2.3 | $\ddot{u}_{i+1} = \zeta^2 u_i - \zeta^2 u_{i+1} + \zeta^2\Delta t\dot{u}_i + \left(\frac{\zeta^2\Delta t^2}{2} + 1\right)\ddot{u}_i$ |
| | **3. *Repeat* 2.1 *to* 2.3 *for the next time steps*** |

* ***M, C,*** *and* ***K*** *are mass, damping, and stiffness matrices, respectively.*
***P****i is the dynamic external load at ith step.*
*N is the number of degree-of-freedom.*

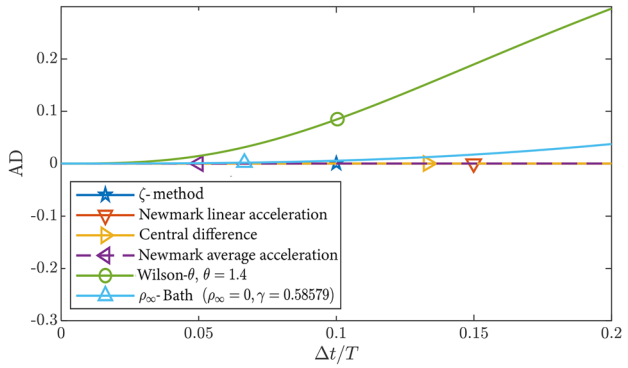


**Figure 10.** Comparing the amplitude decay of the $\zeta$-method for $\zeta = 62.8/\Delta t$ with those of the other time integration methods.

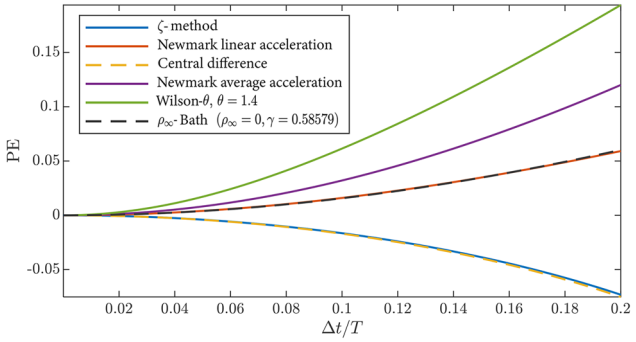


**Figure 11.** Comparing the period elongation of the $\zeta$-method for $\zeta = 62.8/\Delta t$ with those of the other time integration methods.

truncation error. The local truncation error for displacement is defined as follows:

$$e_{u_t+\Delta t} = u(t + \Delta t) - u_{t+\Delta t}, \tag{48}$$

where $u(t + \Delta t)$ is the exact displacement value at time instant $t + \Delta t$, and $u_{t+\Delta t}$ is the displacement value approximated by the time integration method. In general, the time integration method has a consistency order of $p$ if the governing term of the truncation error is of order of $p + 1$. An order of one or greater is required for a method to be consistent [16]. Firstly, the values of displacement, velocity, and acceleration responses at time step $t + \Delta t$ are calculated using Taylor expansion as follows:

$$u(t + \Delta t) = u(t) + \Delta t\dot{u}(t) + \frac{1}{2}\Delta t^2\ddot{u}(t) + \frac{1}{6}\Delta t^3u^{(3)}(t) + R_1(\Delta t^4), \tag{49}$$

$$\dot{u}(t + \Delta t) = \dot{u}(t) + \Delta t\ddot{u}(t) + \frac{1}{2}\Delta t^2u^{(3)}(t) + \frac{1}{6}\Delta t^3u^{(4)}(t) + R_2(\Delta t^4), \tag{50}$$

$$\ddot{u}(t + \Delta t) = \ddot{u}(t) + \Delta tu^{(3)}(t) + \frac{1}{2}\Delta t^2u^{(4)}(t) + \frac{1}{6}\Delta t^3u^{(5)}(t) + R_3(\Delta t^4). \tag{51}$$

where $R_i$s are the residuals and $u^{(n)}(t)$ denotes the $n$th derivative of $u$ with respect to $t$. Moreover, the displacement approximated by $\zeta$-method in Eq. (8) is used as $u_{t+\Delta t}$ for the time step $t+\Delta t$:

$$u_{t+\Delta t}=u(t)+\dot{u}(t)\Delta t+\ddot{u}(t)\frac{\Delta t^2}{2}-\frac{\ddot{u}(t+\Delta t)-\ddot{u}(t)}{\zeta^2}. \quad (52)$$

Then, Eq. (48) is expanded using Eq. (49) for $u(t+\Delta t)$, $u_{t+\Delta t}$ is replaced by Eq. (52), and $\zeta$ is replaced by $C/\Delta t$ as follows:

$$e_{u_{t+\Delta t}}=u(t)+\Delta t\dot{u}(t)+\frac{1}{2}\Delta t^2\ddot{u}(t)+\frac{1}{6}\Delta t^3u^{(3)}(t)+R_1(\Delta t^4)-\left(u(t)+\Delta t\dot{u}(t)+\ddot{u}(t)\frac{\Delta t^2}{2}-\frac{\ddot{u}(t+\Delta t)-\ddot{u}(t)}{(C/\Delta t)^2}\right). \quad (53)$$

In this equation, $\ddot{u}(t+\Delta t)$ is substituted by its Taylor expansion of Eq. (51). After rearranging, the following equation is obtained:

$$e_{u_t+\Delta t}=\left(\frac{1}{6}+\frac{1}{C^2}\right)u^{(3)}(t)\Delta t^3+\frac{1}{2C^2}u^{(4)}(t)\Delta t^4+R(\Delta t^4)+\frac{1}{6C^2}\frac{1}{6}u^{(5)}(t)\Delta t^5+\frac{\Delta t^2}{C^2}R(\Delta t^4). \quad (54)$$

The leading term in the displacement local truncation error of $\zeta$-method is:

$$e_3=\left(\frac{1}{6}+\frac{1}{C^2}\right)u^{(3)}(t)\Delta t^3. \quad (55)$$

In general, it can be stated that the leading term of the displacement local truncation error of the $\zeta$-method is a function of $\Delta t^3$. Taking $C=62.8$, the preceding equation approximately reduces to:

$$e_3=\frac{u^{(3)}(t)}{6}\Delta t^3, \quad (56)$$

which is the leading term of the displacement local truncation error of the $\zeta$-method with $\zeta=62.8/\Delta t$.

Here, the consistency of the velocity solution is also investigated. Since the equation of motion is a second order ordinary differential equation, the single-step time integration method must be also consistent in velocity [16]. The same as displacement, the local truncation error of velocity is defined as follows:

$$e_{\dot{u}_{t+\Delta t}}=\dot{u}(t+\Delta t)-\dot{u}_{t+\Delta t} \quad (57)$$

where $\dot{u}(t+\Delta t)$ is the exact velocity value at time instant $t+\Delta t$ and $\dot{u}_{t+\Delta t}$ is the velocity value approximated by the time integration method. The velocity approximated by $\zeta$-method in Eq. (6) is used as $\dot{u}_{t+\Delta t}$ at the time step $t+\Delta t$:

$$\dot{u}_{t+\Delta t}=\dot{u}(t)+\ddot{u}(t)\Delta t-\frac{\ddot{u}(t+\Delta t)-\ddot{u}(t)}{\zeta\tan(\zeta\Delta t)}. \quad (58)$$

Eq. (57) is expanded using Eq. (50) for $\dot{u}(t+\Delta t)$, $\dot{u}_{t+\Delta t}$ is replaced by Eq. (58), and $\zeta$ is replaced by $C/\Delta t$ as follows:

$$e_{\dot{u}_{t+\Delta t}}=\dot{u}(t)+\Delta t\ddot{u}(t)+\frac{1}{2}\Delta t^2u^{(3)}(t)+\frac{1}{6}\Delta t^3u^{(4)}(t)+R_2(\Delta t^4)-\left(\dot{u}(t)+\ddot{u}(t)\Delta t-\frac{\ddot{u}(t+\Delta t)-\ddot{u}(t)}{(C/\Delta t)\tan(C)}\right). \quad (59)$$

In this equation, $\ddot{u}(t+\Delta t)$ is substituted by its Taylor expansion of Eq. (51). After rearranging and taking $\beta=C\tan(C)$, the following equation is obtained:

$$e_{\dot{u}_{t+\Delta t}}=\left(\frac{1}{\beta}+\frac{1}{2}\right)u^{(3)}(t)\Delta t^2+\left(\frac{1}{2\beta}+\frac{1}{6}\right)u^{(4)}(t)\Delta t^3+\frac{1}{6\beta}u^{(5)}(t)\Delta t^4+R_2(\Delta t^4)+\frac{1}{\beta}\Delta tR_3(\Delta t^4). \quad (60)$$

The leading term in the velocity local truncation error of $\zeta$-method is:

$$e_2=\left(\frac{1}{\beta}+\frac{1}{2}\right)u^{(3)}(t)\Delta t^2, \quad (61)$$

Finally, it can be stated that the leading term of the velocity local truncation error of the $\zeta$-method is a function of $\Delta t^2$.

## 7. Illustrative examples

In this section, some numerical examples are presented and the accuracy of the $\zeta$-method is compared with other time integration methods. For this purpose, some cumulative absolute relative errors are defined as follows:

$$\text{Error}_u(t)=\int_0^t\left|u(\tau)-u_{\text{precise}}(\tau)\right|d\tau\ |,$$
$$\text{Error}_v(t)=\int_0^t\left|\dot{u}(\tau)-\dot{u}_{\text{precise}}(\tau)\right|d\tau, \quad (62)$$
$$\text{Error}_a(t)=\int_0^t\left|\ddot{u}(\tau)-\ddot{u}_{\text{precise}}(\tau)\right|d\tau.$$

where $u(\tau)$, $\dot{u}(\tau)$, and $\ddot{u}(\tau)$ are the displacement, velocity, and acceleration responses, respectively, and $u_{precise}(\tau)$, $\dot{u}_{precise}(\tau)$, and $\ddot{u}_{precise}(\tau)$ are the corresponding precise responses. The integrals were calculated numerically using the trapezoidal method [36]. These errors are used to compare the accuracy of different methods with respect to the precise solutions.

### *7.1. Undamped free vibration*

The free vibration response of an undamped SDOF system was calculated using the $\zeta$-method and was compared with that of the Newmark linear acceleration method and the $\rho_\infty$-Bathe method ($\rho_\infty=0$ and $\gamma=\frac{2-\sqrt{2+2\rho_\infty}}{1-\rho_\infty}$) in Figure 12(a) for the first three cycles using $\Delta t/T=0.1$.

The time variations of the relative displacement cumulative error of Eq. (62) ($Error_u$) for the three methods are illustrated in Figure 12(b). In this equation, $u_{precise}(\tau)$ is taken as the exact theoretical solution for the undamped free vibration. The results show that in terms of accuracy, $\rho_\infty$-

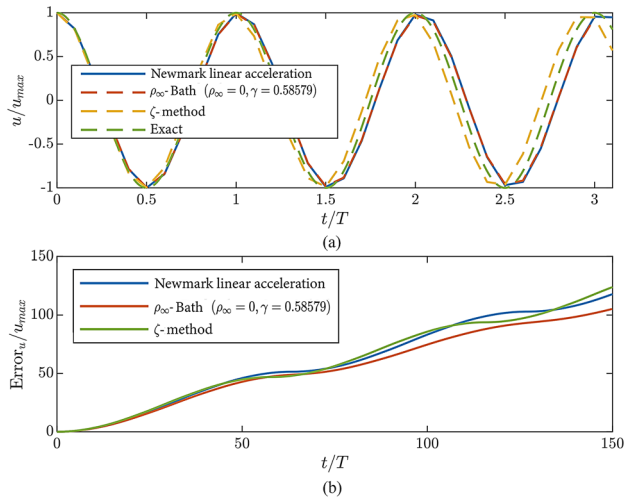


**Figure 12.** (a) The first three cycles of free vibration responses; (b) the cumulative displacement error of an undamped SDOF system with $\Delta t/T = 0.1$ using the Newmark linear acceleration, $\rho_\infty$-Bathe, and the $\zeta$-method.

Bathe method has the least error while Newmark linear acceleration and $\zeta$-method are almost the same (at different cycles behave differently). In addition, it is obvious that the $\zeta$-method is an implicit method with period shrinkage, while the Newmark linear acceleration and the $\rho_\infty$-Bathe methods cause period elongation.

### *7.2. Response of a short-period system subjected to El Centro record*

To evaluate the performance of the $\zeta$-method in earthquake engineering, the dynamic response of a damped SDOF system with a natural period of 0.2 sec and damping ratio of $\xi = 0.05$ was investigated. The unscaled record of the El Centro ground motion during Imperial Valley earthquake of 1940 was chosen as the input acceleration with a time step of $\Delta t = 0.02$ sec, resulting in a $\Delta t/T = 0.1$. Using $g = 9806\ \text{mm/sec}^2$, the dynamic response was calculated using the $\zeta$-method.

To find a precise solution, each time step of the record was divided into ten sub-steps and the corresponding amplitudes were obtained using linear interpolation ($\Delta t = 0.002$ sec and $\Delta t/T = 0.01$) which resulted in almost the same responses for all methods.

The process was repeated for the original record ($\Delta t = 0.02$ sec) for $\zeta$-method, Newmark linear acceleration method, and $\rho_\infty$-Bathe method ($\rho_\infty = 0$ and $\gamma = \frac{2-\sqrt{2+2\rho_\infty}}{1-\rho_\infty}$) and the responses were compared with the precise solution. This comparison for the displacement, velocity and acceleration responses has been illustrated in Figure 13 revealing the accuracy of the method.

Since the $\rho_\infty$-Bathe method is a sub-step method, it obviously represents the highest accuracy. On the other hand, in terms of execution time, the $\rho_\infty$-Bathe method is significantly more time-consuming than the $\zeta$-method. To provide a fair comparison basis, an interpolated version of the $\zeta$-method was used using a linear interpolation of the input load for $\Delta t_{interpolation} = \Delta t/2$. By this, the execution time of both methods got closer and using the linear interpolation, two sub-steps were generated at each time step of the $\zeta$-method (equal to that of $\rho_\infty$-Bathe). The response of the interpolated version of the $\zeta$-method is denoted as "$\zeta$-method (interpolated)" in Figure 13.

The plot of the cumulative relative error for displacement of Eq. (62) with respect to time is illustrated in Figure 14(a). Taking $T$ as the duration of the input excitation, the total errors are defined as $Error_u(T)$, $Error_v(T)$, and $Error_a(T)$. The total errors and the execution times of $\zeta$-method (interpolated), $\zeta$-method, $\rho_\infty$-Bathe method ($\rho_\infty = 0$ and $\gamma = \frac{2-\sqrt{2+2\rho_\infty}}{1-\rho_\infty}$), and Newmark linear acceleration method are given in Table 4. Moreover, the mean-value of execution time for 1,000 executions is reported for each method in Table 4. It is observed that the total displacement error of the interpolated $\zeta$-method is one-third that of $\rho_\infty$-Bathe with an equal execution time.

To assess the effect of the natural period of vibration on the accuracy, the total displacement error of the methods was calculated for different periods and normalized to the cumulative absolute value of the precise displacement response (i.e., $\int_0^T \left|u_{\text{precise}}(\tau)\right| d\tau\Big)$) with the same period. For this purpose, the displacement response under the El Centro ground motion with $\Delta t = 0.02$ sec was obtained for several natural periods using different time integration methods. Figure 14(b) represents this comparison revealing the fact that the interpolated $\zeta$-method has the lowest error for different natural periods and consequently different $\Delta t/T$ values. Moreover, the Newmark linear acceleration method and the $\zeta$-method are almost similar in terms of error.

### *7.3. A long-period system under a harmonic loading*

Figure 15 presents the displacement, velocity, and acceleration responses of an undamped SDOF system subjected to a harmonic force. The force function was selected as $P(t) = p_0 \sin(\Omega t)$ with $\Omega = 3$ rad/sec and $p_0 = 1000$ N/m. The initial displacement and velocity were taken as zero and the system stiffness ($k$) and mass ($m$) were 622.22 N/m and 96 kg, respectively, resulting in a period of 2.468 sec. The exact solution and the numerical response of the system using the interpolated version of $\zeta$ -method ($\Delta t_{interpolation} = \Delta t/2$), $\zeta$-method, $\rho_\infty$-Bathe method, and Newmark linear acceleration method were compared when $\Delta t = 0.2$ sec . It is observed that the $\zeta$-method showed more accurate results than the Newmark linear acceleration and the $\rho_\infty$-Bathe method in the case of a long-period system.

The time variation of $Error_u(t)$ is plotted in Figure 16 and the total errors and the mean-value of the execution times of the time-stepping process are given in Table 5. It is observed that $\zeta$-method is more accurate than both Newmark linear acceleration

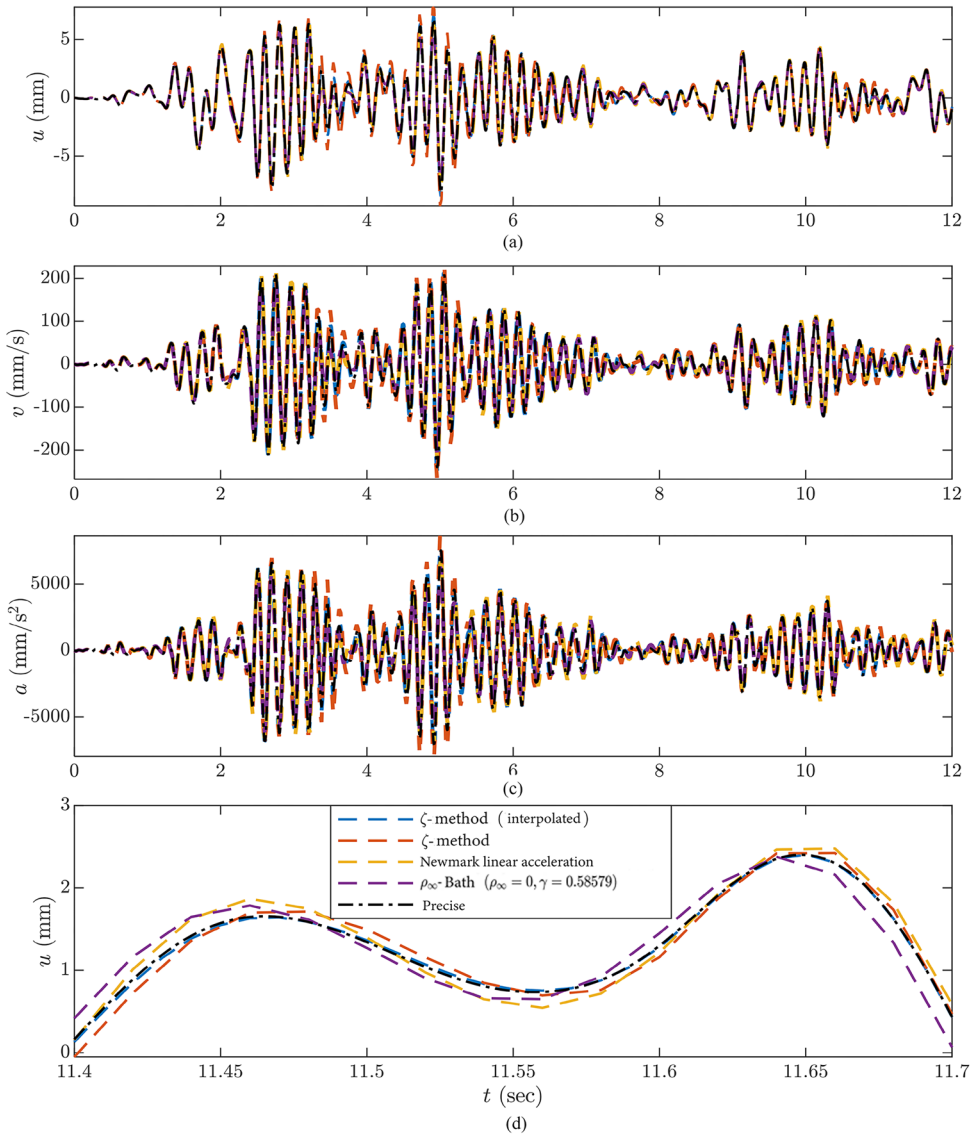


**Figure 13.** Comparing the responses of ζ-method (interpolated), ζ-method, Newmark linear acceleration method, and $\rho_\infty$-Bathe method ($\Delta t$ = 0.02 sec) with the precise response ($\Delta t$ = 0.002 sec) under El Centro record: (a) displacement response; (b) velocity response; (c) acceleration reponse; and (d) close-up of displacement response.

**Table 4 .**The comparison of the total absolute relative error and the execution time of different methods for a SDOF system with $T$ = 0.2 sec subjected to El Centro ground motion.

| Method | Total displacement error (mm.sec) | Total velocity error (mm) | Total acceleration error (mm/sec) | Execution time (milliseconds) |
|---|---|---|---|---|
| ζ-method (interpolated) | 2.09 | 62.73 | 2036.92 | 0.0690 |
| ζ-method | 8.56 | 251.79 | 8335.76 | 0.0190 |
| Newmark linear acceleration | 7.33 | 232.29 | 7267.04 | 0.0262 |
| ρ∞-Bathe | 6.30 | 194.24 | 6259.01 | 0.0771 |

**Table 5.** Comparison of the total error and the execution time of different methods.

| Method | Total displacement error (m.sec) | Total velocity error (m) | Total acceleration error (m/sec) | Execution time (milliseconds) |
|---|---|---|---|---|
| ζ-method (interpolated) | 1.663 | 3.770 | 10.780 | 0.0034 |
| ζ-method | 5.370 | 13.441 | 34.835 | 0.0018 |
| Newmark linear acceleration | 5.752 | 16.165 | 37.038 | 0.0018 |
| ρ∞-Bathe | 6.304 | 24.215 | 56.070 | 0.0040 |

method and $\rho_\infty$-Bathe method. For the displacement response, interpolated ζ-method is five times more accurate than the $\rho_\infty$-Bathe method with a nearly equal execution time for the long period system under a harmonic loading.

### *7.4. A nonlinear SDOF system*

The numerical responses of a nonlinear SDOF system subjected to a harmonic load were compared for different methods as shown in Figure 17(a). The SDOF system had a

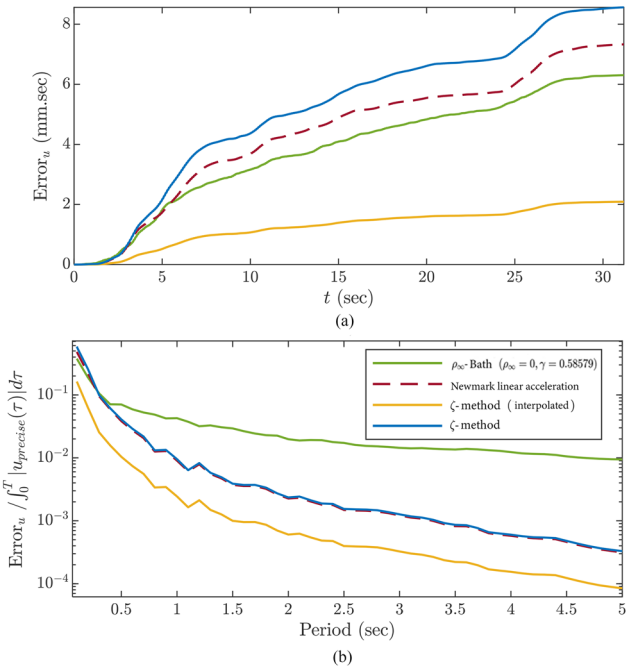


**Figure 14.** (a) The cumulative absolute relative displacement error of several methods for a SDOF system with $T = 0.2$ sec; (b) the normalized total displacement error of several methods for systems with different natural periods subjected to El Centro record.

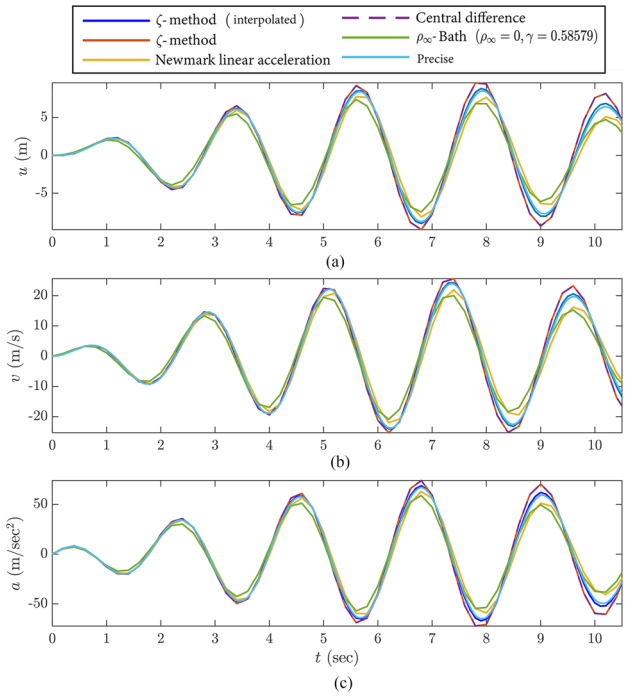


**Figure 15.** The response of an undamped SDOF system with $T = 2.468$ sec and $\Delta t = 0.2$ sec subjected to $P = 1000 \sin(3t)$: (a) displacement response; (b) velocity response; and (c) acceleration reponse.

mass of $m = 0.2533$ kg, a stiffness of $k = 10$ N/m (a period of 1sec ), and a damping ratio of $\xi = 0.05$. An elasto-plastic behavior was considered for the system with a yielding force of 10 N. A harmonic load equal to $P(t) = 10\sin(2\pi t)/0.6$ was applied to the system from time instant 0 to 0.5 sec with no initial conditions. The response for

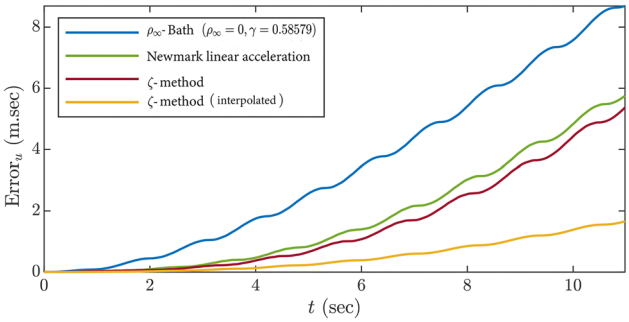


**Figure 16.** The cumulative relative displacement error of several methods of an undamped SDOF system subjected to the harmonic force of $P = 1000 \sin(3t)$.

10 sec was calculated and to solve the nonlinear response, Newton-Raphson iteration was also used [1, 36]. The time step for the numerical solution was taken equal to $\Delta t = 0.1$ sec. To find the precise response as a reference for comparison, the response was once calculated using a time step equal to $\Delta t = 0.01$ sec using Newmark linear acceleration method. The numerical response of the system using different methods were compared with the precise response.

The time variation of $Error_u(t)$ of Eq. (62) is plotted in Figure 17(b) and the total errors are given in Table 6. The results showed that $\zeta$-method was more accurate than the Newmark linear and average acceleration methods for the displacement response, while it was almost the same in terms of velocity and acceleration errors.

### *7.5. A multi-degree-of-freedom system*

The shear building of Figure 18, which is taken from Section 12.1 of reference [1] (with modifications), is used to investigate the accuracy of the $\zeta$-method as a MDOF system. The mass ($M$) and stiffness ($K$) matrices and the input dynamic load are defined in Figure 18. For this system, $m = 2.5880$ kg, $k = 100$ N/m, $\ddot{u}_g = 193.2\sin(2\pi t)$, and the loading function $P(t)$ was applied from time instant 0 to 1sec with no initial conditions.

A constant damping ratio of $\xi = 0.05$ was considered for all modes and the damping matrix was calculated accordingly. The modal periods were calculated as $T_n = [3.5512;\ 1.2166;\ 0.7718;\ 0.6008;\ 0.5267]$sec, resulting in $\Delta t/T_n = [0.0282;\ 0.0822;\ 0.1296;\ 0.1665;\ 0.1898]$. The dynamic responses for all DOFs were calculated for 10 sec, and the time step for the numerical solution was taken equal to $\Delta t = 0.1$ s. To find the precise responses, the solution was once calculated using a time step equal to $\Delta t = 0.001$ sec using Newmark linear acceleration method. The numerical solutions for $\zeta$-method, Newmark linear acceleration, and Newmark average acceleration methods were compared with the precise responses as represented in Figure 19.

**Table 6.** Comparison of the total error of different methods.

| Method | Total displacement error (m.sec) | Total velocity error (m) | Total acceleration error (m/sec) |
|---|---|---|---|
| ζ-method | 0.72743 | 40.339 | 90.435 |
| Newmark linear acceleration | 1.958 | 37.842 | 89.13 |
| Newmark average acceleration | 3.2004 | 36.674 | 88.418 |

**Table 7.** Comparison of the total error of different methods.

| *Method* | Total $Error_u$ (m. sec) | Total $Error_v$ (m) | Total $Error_a$ (m/sec) | Total $Error_u$ (m. sec) | Total $Error_v$ (m) | Total $Error_a$ (m/sec) |
|---|---|---|---|---|---|---|
| ***DOF*** | | $u_1$ | | | $u_2$ | |
| *ζ-method* | 2.828065 | 15.97523 | 116.6835 | 3.72312 | 16.7361 | 93.0644 |
| *Newmark linear acceleration* | 5.139863 | 28.7022 | 193.7407 | 6.44375 | 31.62849 | 168.6993 |
| *Newmark average acceleration* | 2.899619 | 15.45146 | 108.7588 | 3.77382 | 16.8867 | 88.6841 |
| ***DOF*** | | $u_3$ | | | $u_4$ | |
| *ζ-method* | 3.748271 | 15.27157 | 104.7166 | 4.11576 | 10.9837 | 69.64 |
| *Newmark linear acceleration* | 5.741478 | 25.24164 | 167.8254 | 6.21416 | 17.97887 | 116.8667 |
| *Newmark average acceleration* | 4.07242 | 14.697 | 93.1223 | 5.06203 | 12.3865 | 67.4613 |
| ***DOF*** | | $u_5$ | | | | |
| *ζ-method* | 5.007442 | 17.66328 | 109.149 | | | |
| *Newmark linear acceleration* | 8.186316 | 33.53575 | 188.2962 | | | |
| *Newmark average acceleration* | 6.079406 | 18.96263 | 101.2013 | | | |

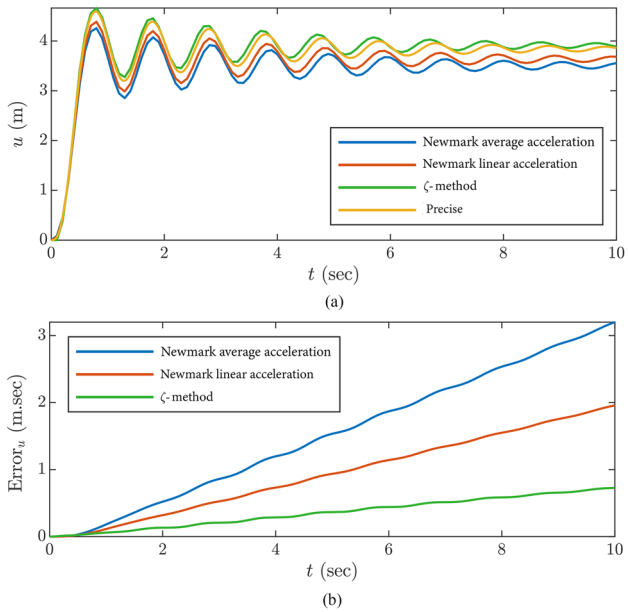


**Figure 17.** (a) the nonlinear displacement response; (b) the cumulative relative displacement error of different time integration methods of the nonlinear SDOF system with $T = 1$ sec and $\Delta t = 0.1$ sec subjected to $P(t) = 10 \sin(2\pi t)/0.6$.

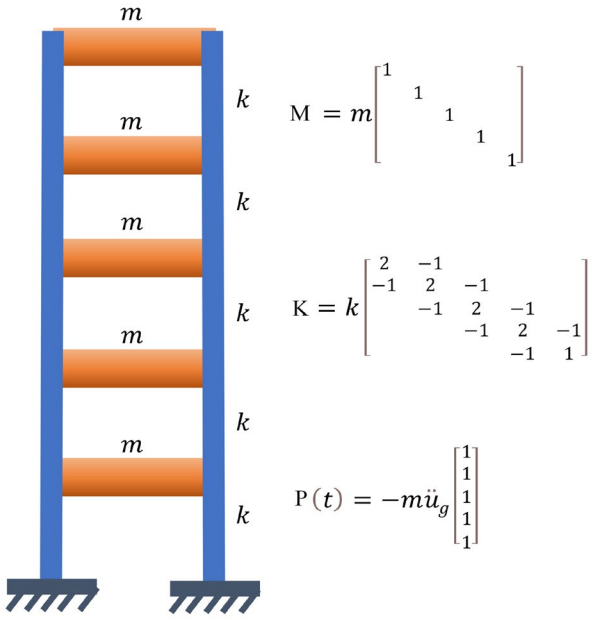


**Figure 18.** Shear building of Example 7.5 with mass and stiffness matrices, and the input dynamic load.

The cumulative displacement error of Eq. (62) is illustrated in Figure 20, and the total errors are given in Table 7. The results showed that for this example, the $\zeta$-method was more accurate than the Newmark linear and average acceleration methods for the displacement response. In addition, for the velocity and acceleration responses, $\zeta$-method is more accurate than linear acceleration method while it is almost the same as the average acceleration method. It is worth mentioning that for the higher modes with more critical $\Delta t/T_n$s, the accuracy of the $\zeta$-method was significant.

It should be noted that since an effective time integration method should be able to deal with large-scale dynamic systems involving many degrees of freedom, for future studies it is suggested to investigate the accuracy and performance of the proposed method for large-scale problems [38-40].

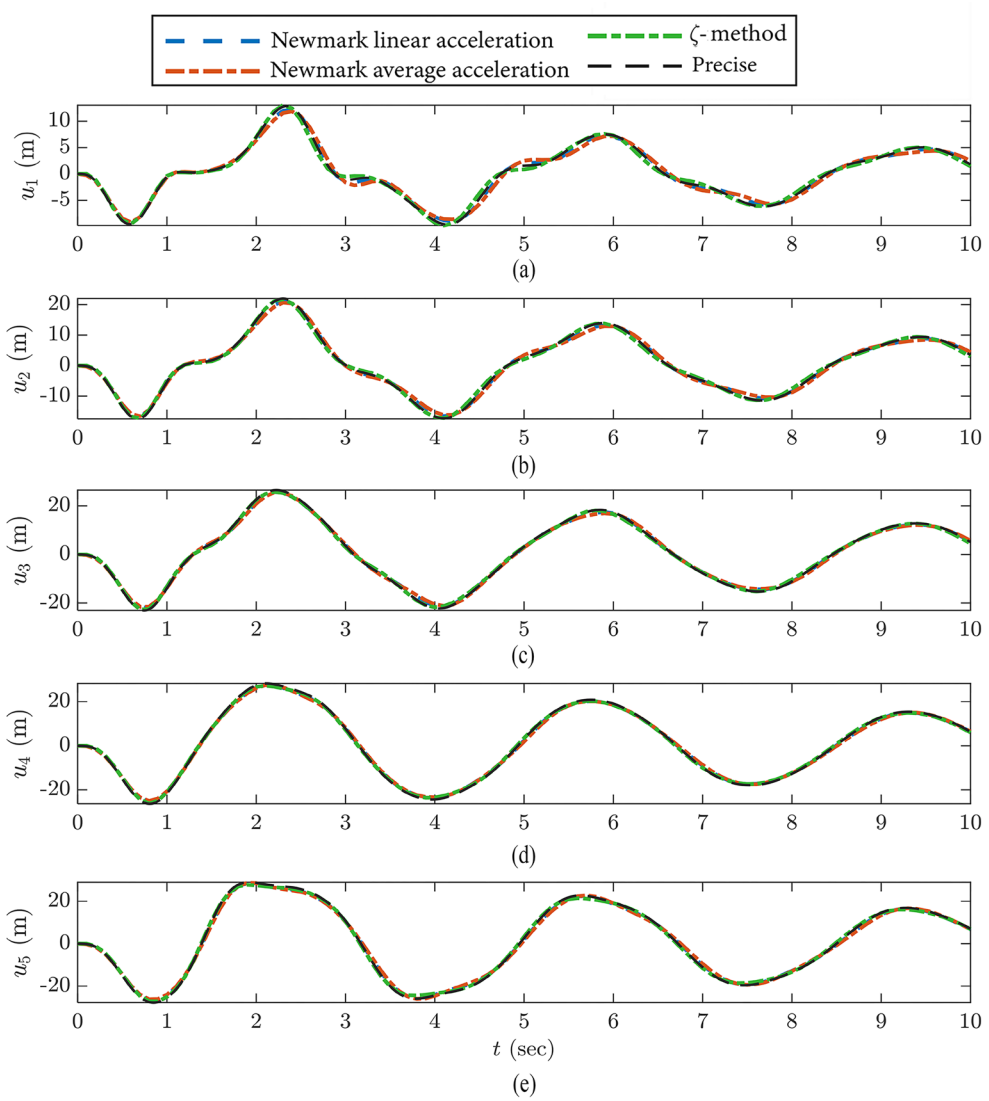


**Figure 19.** The numerical displacement responses of: a) first; b) second; c) third; d) fourth; and e) fifth DOFs of the MDOF system with $\Delta t$ = 0.1 sec subjected to harmonic load.

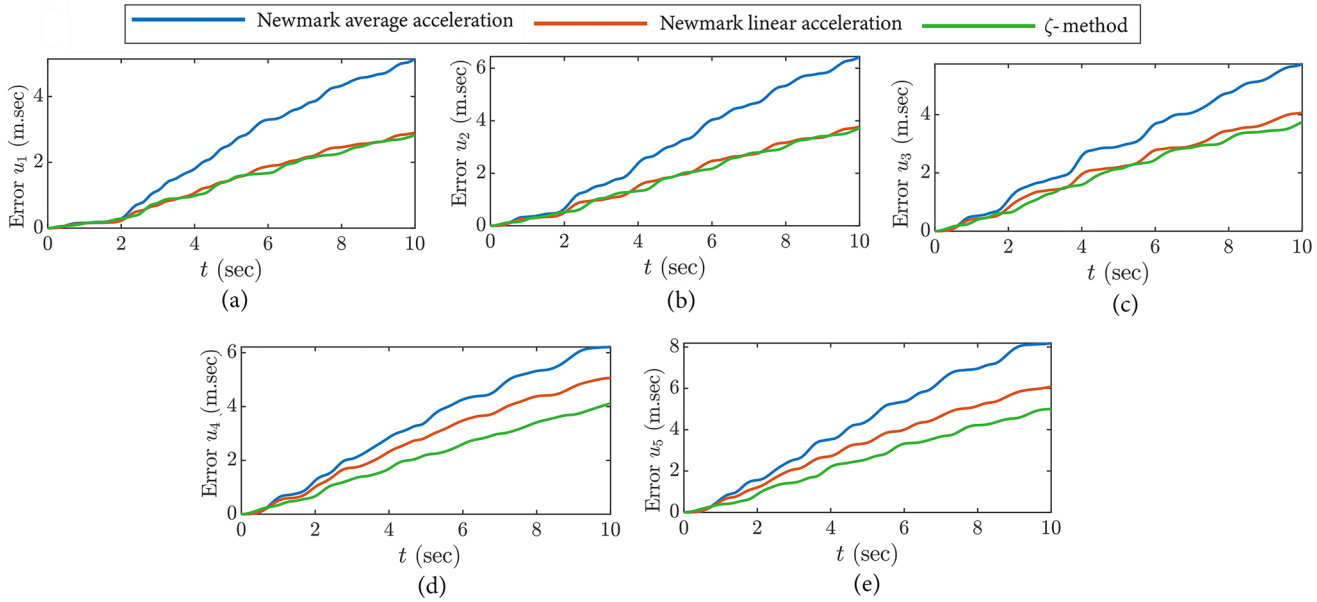


**Figure 20** The cumulative relative displacement error of different time integration methods of the MDOF system subjected to the harmonic load.

## 8. Conclusions

An implicit numerical technique, named $\zeta$-method, was introduced for solving the equation of motion of dynamic systems. The method assumes a sinusoidal distribution for the response acceleration between two successive time steps. In the formulation of the method, a parameter $\zeta$ was defined which prescribes the frequency of the interpolation function, the amplitude decay, the period elongation, and indeed, the accuracy of the method. The best value for parameter $\zeta$ was obtained by minimizing the amplitude decay and the period elongation using multi-objective optimization technique. According to the analysis results, $\zeta = 62.8/\Delta t$ offers the best accuracy.

Moreover, accuracy, stability, spectral radius, consistency, and performance of the method were theoretically and numerically discussed. Accordingly, the $\zeta$-method is a conditionally stable time integration method with slight period shrinkage. This method was stable for $\Delta t/T < 0.3$ and could be confidently and efficiently used for $\Delta t/T < 0.1$ to obtain highly accurate responses.

In addition, an interpolated version of the $\zeta$-method was also introduced which showed significant accuracy in comparison with similar methods. A few problems were also solved using both versions of the method and the results were compared with those of well-known and recently developed technics. The $\zeta$-method had superior results and performances for the long-period system under harmonic loading, the nonlinear structure, and the Multi-Degree-of-Freedom (MDOF) system examined in this paper.

In this work, the focus was centered on the development of the formulations to form the basis of the $\zeta$-method considering the implicit scheme. Further studies on the $\zeta$-method with more sinusoidal terms as the acceleration interpolation function, and mathematical derivation of the interpolated version of the $\zeta$-method could be very useful. Moreover, since an effective time integration method should be able to deal with large-scale dynamic systems involving many degrees of freedom, for future studies it is suggested to investigate the accuracy and performance of the $\zeta$-method for large-scale problems.

## Funding

This research did not receive any specific grant from funding agencies in the public, commercial, or not-for profit sectors.

## Conflicts of interest

The authors declare that they have no known competing financial interests or personal relationships that could have appeared to influence the work reported in this paper.

## Authors contribution statement

**First author**
Soroosh Kamali: Conceptualization; Data curation; Formal analysis; Investigation; Methodology; Software; Validation; Writing – original draft.

**Second author**
Seyed Mehdi Dehghan: Conceptualization; Methodology; Project administration; Resources; Supervision; Validation; Writing – review and editing.

**Third author**
Mohammad Amir Najafgholipour: Investigation; Methodology; Writing – review and editing.

**Fourth author**
Mohammad Ali Hadianfard: Investigation; Methodology; Writing – review and editing.

## References

1. Chopra, A.K., *Dynamics of Structures*, 4th Ed., Prentice Hall (2012).

2. Houbolt, J.C. "A recurrence matrix solution for the dynamic response of elastic aircraft", *Journal of the Aeronautical Sciences*, **17**(9), pp. 540-550 (1950). https://doi.org/10.2514/8.1722

3. Newmark, N.M. "A method of computation for structural dynamics", *Journal of the Engineering Mechanics Devision ASCE*, **85**(3), pp. 67-94 (1959). https://doi.org/10.1061/JMCEA3.0000098

4. Wilson, E.L., Farhoomand, I., and Bathe, K.J. "Nonlinear dynamic analysis of complex structures", *Earthquake Engineering and Structural Dynamics*, **1**(3), pp. 241-252 (1972). https://doi.org/10.1002/eqe.4290010305

5. Leontyev, V. "Direct time integration algorithm with controllable numerical dissipation for structural dynamics: Two-step Lambda method", *Applied Numerical Mathematics*, **60**(3), pp. 277-292 (2010). https://doi.org/10.1016/j.apnum.2009.12.005

6. Bathe, K.J. and Noh, G. "Insight into an implicit time integration scheme for structural dynamics", *Computers and Structures*, **98**, pp. 1-6 (2012). https://doi.org/10.1016/j.compstruc.2012.01.009

7. Noh, G. and Bathe, K.J. "Further insights into an implicit time integration scheme for structural dynamics", *Computers & Structures*, **202**, pp. 15-24 (2018). https://doi.org/10.1016/j.compstruc.2018.02.007

8. Wen, W.B., Jian, K.L., and Luo, S.M. "An explicit time integration method for structural dynamics using septuple B-spline functions", *International Journal for Numerical Methods in Engineering*, **97**(9), pp. 629-657 (2014). https://doi.org/10.1002/nme.4599

9. Wen, W.B., Luo, S.M., and Jian, K.L. "A novel time integration method for structural dynamics utilizing uniform quintic B-spline functions", *Archive of Applied Mechanics*, **85**(12), pp. 1743-1759 (2015). https://doi.org/10.1007/s00419-015-1016-5

10. Rostami, S., Shojaee, S., and Saffari, H. "An explicit time integration method for structural dynamics using cubic B-spline polynomial functions", *Scientia Iranica*, **20**(1), pp. 23-33 (2013). https://doi.org/10.1016/j.scient.2012.12.003

11. Shojaee, S., Rostami, S., and Abbasi, A. "An unconditionally stable implicit time integration algorithm: Modified quartic B-

spline method", *Computers and Structures*, **153**, pp. 98-111 (2015). https://doi.org/10.1016/j.compstruc.2015.02.030

12. Muradova, A.D. "A time spectral method for solving the nonlinear dynamic equations of a rectangular elastic plate", *Journal of Engineering Mathematics*, **92**(1), pp. 83-101 (2015). https://doi.org/10.1007/s10665-014-9752-z

13. Ding, Z., Li, L., Hu, Y., et al. "State-space based time integration method for structural systems involving multiple nonviscous damping models", *Computers and Structures*, **171**, pp. 31-45 (2016). https://doi.org/10.1016/j.compstruc.2016.04.002

14. Hadianfard, M.A. "Using integrated displacement method to time-history analysis of steel frames with nonlinear flexible connections", *Structural Engineering and Mechanics*, **41**(5), pp. 675-689 (2012). https://doi.org/10.1016/j.compstruc.2016.04.002

15. Wen, W.B., Wei, K., Lei, H.S., et al. "A novel sub-step composite implicit time integration scheme for structural dynamics", *Computers and Structures*, **182**, pp. 176-186 (2017). https://doi.org/10.1016/j.compstruc.2016.11.018

16. Zhang, J., Liu, Y., and Liu, D. "Accuracy of a composite implicit time integration scheme for structural dynamics", *International Journal for Numerical Methods in Engineering*, **109**(3), pp. 368-406 (2017). https://doi.org/10.1002/nme.5291

17. Kwon, S.B. and Lee, J.M. "A non-oscillatory time integration method for numerical simulation of stress wave propagations", *Computers and Structures*, **192**, pp. 248-268 (2017). https://doi.org/10.1016/j.compstruc.2017.07.030

18. Xing, Y., Zhang, H., and Wang, Z. "Highly precise time integration method for linear structural dynamic analysis", *International Journal for Numerical Methods in Engineering*, **116**(8), pp. 505-529 (2018). https://doi.org/10.1002/nme.5934

19. Kim, W. and Choi, S.Y. "An improved implicit time integration algorithm: The generalized composite time integration algorithm", *Computers and Structures*, pp. 341-354 (2018). https://doi.org/10.1016/j.compstruc.2017.10.002

20. Zhang, H.M. and Xing, Y.F. "Two novel explicit time integration methods based on displacement-velocity relations for structural dynamics", *Computers and Structures*, **221**, pp. 127-141 (2019). https://doi.org/10.1016/j.compstruc.2019.05.018

21. Yuan, P., Li, D., Cai, C.S., et al. "Time integration method with high accuracy and efficiency for structural dynamic analysis", *Journal of Engineering Mechanics*, **145**(3), 04019008 (2019). https://doi.org/10.1061/(ASCE)EM.1943-7889.0001574

22. Kim, W. "A simple explicit single step time integration algorithm for structural dynamics", *International Journal for Numerical Methods in Engineering*, **119**(5), pp. 383-403 (2019). https://doi.org/10.1002/nme.6054

23. Kim, W. and Reddy, J.N. "Novel explicit time integration schemes for efficient transient analyses of structural problems", *International Journal of Mechanical Sciences***172**, 105429 (2020). https://doi.org/10.1016/j.ijmecsci.2020.105429

24. Noh, G. and Bathe, K.J. "The Bathe time integration method with controllable spectral radius: The $\rho_\infty$-Bathe method", *Computers & Structures*, **212**, pp. 299-310, (2019). https://doi.org/10.1016/j.compstruc.2018.11.001

25. Malakiyeh, M.M., Shojaee, S., and Bathe, K.J. "The Bathe time integration method revisited for prescribing desired numerical dissipation", *Computers and Structures*, **212**, pp. 289-298 (2019). https://doi.org/10.1016/j.compstruc.2018.10.008

26. Li, J. and Yu, K. "A novel family of composite sub-step algorithms with desired numerical dissipations for structural dynamics", *Archive of Applied Mechanics*, **90**(4), pp. 737-772 (2020).

27. Nguyen, D.T., Li, L., and Ji, H. "Stable and accurate numerical methods for generalized Kirchhoff–Love plates", *Journal of Engineering Mathematics*, **130**(1), pp. 1-26 (2021). https://doi.org/10.1007/s10665-021-10163-x

28. Subbaraj, K. and Dokainish, M.A. "A survey of direct time-integration methods in computational structural dynamics-II. Implicit methods", *Computers and Structures*, **32**(6), pp. 1387-1401 (1989).

29. Mosqueda, G. and Ahmadizadeh, M. "Iterative implicit integration procedure for hybrid simulation of large nonlinear structures", *Earthquake Engineering and Structural Dynamics*, **40**(9), pp. 945-960 (2011). https://doi.org/10.1002/eqe.1066

30. Jia, C., Bursi, O.S., Bonelli, A., et al. "Novel partitioned time integration methods for DAE systems based on L-stable linearly implicit algorithms", *International Journal for Numerical Methods in Engineering*, **87**(12), pp. 1148-1182 (2011). https://doi.org/10.1002/nme.3153

31. Ohno, N., Tsuda, M., and Kamei, T. "Elastoplastic implicit integration algorithm applicable to both plane stress and three-dimensional stress states", *Finite Elements in Analysis and Design*, **66**, pp. 1-11 (2013). https://doi.org/10.1016/j.finel.2012.11.001

32. Zhang, H., Zhang, R., Zanoni, A., et al. "Performance of implicit A-stable time integration methods for multibody system dynamics", *Multibody System Dynamics*, **54**(3), pp. 263-301 (2022). https://doi.org/10.1007/s11044-021-09806-9

33. Dokainish, M.A. and Subbaraj, K. "A survey of direct time-integration methods in computational structural dynamics-I. Explicit methods", *Computers & Structures*, **32**(6), pp. 1371-1386 (1989). https://doi.org/10.1016/0045-7949(89)90314-3

34. Chang, S.Y. "Explicit pseudodynamic algorithm with unconditional stability", *Journal of Engineering Mechanics*, **128**(9), pp. 935-947 (2002). https://doi.org/10.1061/(ASCE)0733-9399(2002)128:9(935)

35. Hulbert, G.M. and Chung, J. "Explicit time integration algorithms for structural dynamics with optimal numerical dissipation", *Computer Methods in Applied Mechanics and Engineering*, **137**(2), pp. 175-188 (1996). https://doi.org/10.1061/(ASCE)0733-9399(2002)128:9(935)

36. Humar, J. *Dynamics of Structures*, CRC press, (2012). https://doi.org/10.1201/b11772

37. Coello, C.C. and Lechuga, M.S. "MOPSO: A proposal for multiple objective particle swarm optimization", *Proceedings of the 2002 Congress on Evolutionary Computation*, Honolulu, (2002). https://doi.org/10.1109/CEC.2002.1004388

38. Zhang, C., Long, K., Yang, X., et al. "A transient topology optimization with time-varying deformation restriction via augmented Lagrange method", *International Journal of Mechanics and Materials in Design*, **18**(3), pp. 1-18 (2022).

https://doi.org/10.1007/s10999-022-09598-6

39. Burlayenko, V.N. and Sadowski, T. "Transient dynamic response of debonded sandwich plates predicted with finite element analysis", *Meccanica*, **49**(11), pp. 2617-2633 (2014). https://doi.org/10.1007/s11012-014-9924-y

40. Long, K., Yang, X., Saeed, N., et al. "Topology optimization of transient problem with maximum dynamic response constraint using SOAR scheme", *Frontiers of Mechanical Engineering*, **16**(3), pp. 593-606, (2021). https://doi.org/10.1007/s11465-021-0636-4

## Biographies

**Soroosh Kamali** is a PhD candidate of earthquake engineering in Shiraz University of Technology and a research fellow of structural health monitoring in University of Bologna. His main research activities center on structural health monitors and damage detection/classification of railway bridges, automated model updating algorithms using artificial intelligence, novel frequency domain modal identification techniques, and numerical methods in dynamics of structures.

**Seyed Mehdi Dehghan** is an Associate Professor in Civil and Environmental Engineering Department at Shiraz University of Technology. He received his BSc and MSc degrees from Shiraz University Shiraz, Iran. Also, he received his PhD degree in structural and earthquake engineering from Tohoku University, Japan, in 2008. His research interests include seismic behavior (numerical and experimental study) of steel, RC, and masonry structures; seismic evaluation of lifeline systems; passive control of structures; and seismic isolation. He has published more than 30 journal papers.

**Mohammad Amir Najafgholipour** is an Associate Professor in the Department of Civil and Environmental Engineering, at Shiraz University of Technology. He received BSc, MSc, and PhD degrees from Shiraz University in 2004, 2007, and 2012, respectively. He also had a sabbatical visit in Minho University, Portugal, in 2011. His main areas of research interest are seismic performance assessment and retrofitting of existing buildings, experimental and numerical studies on masonry and RC structures, structural dynamics, and construction materials. He is now the head of department at Shiraz University of Technology and also serves as a committee member of Iranian National Building Code for Design and Construction of Masonry Buildings.

**Mohammad Ali Hadianfard** was born in Shiraz, Iran, in 1969. He obtained his BSc degree in Civil Engineering from Shiraz University, Iran in 1992. He continued his studies on Structures at Shiraz University, and received his MSc and PhD degrees in 1995 and 2002, respectively. He is currently Full Professor of Civil Engineering in Shiraz University of Technology. He has published about 40 journal papers. Also, he presented about 30 papers in the international and 60 papers in the national conferences. Moreover, he has contributed in writing 10 national standards of Iran. His research interests are: rehabilitation, steel connections and semi-rigid connections, nonlinear analysis, structural reliability, damage detection, progressive collapse.